Publication Year	2017
Acceptance in OA@INAF	2020-08-21T15:52:22Z
Title	Intracluster Patches of Baryons in the Core of the Fornax Cluster
Authors	IODICE, ENRICHETTA; SPAVONE, MARILENA; CANTIELLO, Michele; D'Abrusco, R.; Capaccioli, M.; et al.
DOI	10.3847/1538-4357/aa9b30
Handle	http://hdl.handle.net/20.500.12386/26759
Journal	THE ASTROPHYSICAL JOURNAL
Number	851

The Astrophysical Journal, 851:75 (9pp), 2017 December 20 https://doi.org/10.3847/1538-4357/aa9b30
© 2017. The American Astronomical Society. All rights reserved.

Intracluster Patches of Baryons in the Core of the Fornax Cluster

E. Iodice[1], M. Spavone[1], M. Cantiello[2], R. D'Abrusco[3], M. Capaccioli[4], M. Hilker[5], S. Mieske[6], N. R. Napolitano[1], R. F. Peletier[7], L. Limatola[1], A. Grado[1], A. Venhola[8], M. Paolillo[9], G. Van de Ven[10], and P. Schipani[1]
[1] INAF-Astronomical Observatory of Capodimonte, via Moiariello 16, Naples, I-80131, Italy; iodice@na.astro.it
[2] INAF-Astronomical Observatory of Teramo, Via Maggini, I-64100, Teramo, Italy
[3] Smithsonian Astrophysical Observatory/Chandra X-ray Center, Cambridge, MA 02138, USA
[4] University of Naples "Federico II," C.U. Monte Sant Angelo, Via Cinthia, I-80126, Naples, Italy
[5] European Southern Observatory, Karl-Schwarzschild-Strasse 2, D-85748 Garching bei Munchen, Germany
[6] European Southern Observatory, Alonso de Cordova 3107, Vitacura, Santiago, Chile
[7] Kapteyn Astronomical Institute, University of Groningen, P.O. Box 72, 9700 AV Groningen, The Netherlands
[8] Division of Astronomy, Department of Physics, University of Oulu, Oulu, Finland
[9] Univ. of Naples "Federico II," C.U. Monte Sant Angelo, Via Cinthia, I-80126, Naples, Italy
[10] Max Planck Institute for Astronomy, Heidelberg, Germany
Received 2017 July 18; revised 2017 November 10; accepted 2017 November 10; published 2017 December 14

Abstract

In the core of the Fornax cluster, on the west side of NGC 1399, we have detected a previously unknown region of intracluster light (ICL). It is made up by several faint ($\mu_r \simeq$ 28–29 mag arcsec^{-2}) patches of diffuse light. The bulk of the ICL is located in between the three bright galaxies in the core, NGC 1387, NGC 1379, and NGC 1381, at $10 \leqslant R \leqslant 40$ arcmin (∼58–230 kpc) from the central galaxy NGC 1399. We show that the ICL is the counterpart in the diffuse light of the known over-density in the population of blue globular clusters (GCs). The total g-band luminosity of the ICL is $L_g \simeq 8.3 \times 10^9\ L_\odot$, which is ∼5% of the total luminosity of NGC 1399. This is consistent with the fraction of the blue GCs in the same region of the cluster. The ICL has $g - r \sim 0.7$ mag, which is similar to the colors in the halo of the bright galaxies in the cluster core. The new findings were compared with theoretical predictions for the ICL formation and they support a scenario in which the intracluster population detected in the core of the Fornax cluster is build up by the tidal stripping of material (stars and GCs) from galaxy outskirts in a close passage with the central brightest galaxy (cD). Moreover, the diffuse form of the ICL and its location close to the core of the cluster is expected in a dynamically evolved cluster like Fornax.

Key words: galaxies: clusters: intracluster medium – galaxies: interactions

1. Introduction

Many studies have proved the existence of intracluster baryons, in stars and GCs, which are not gravitationally bound to any of the cluster members (Zibetti et al. 2005; Gonzalez et al. 2007; Arnaboldi & Gerhard 2010; Tutukov & Fedorova 2011; Mihos 2015). The intracluster light (ICL) is the diffuse component from the starlight that contributes to the surface brightness (SB) profile of the bright cluster galaxy (BCG) at magnitudes fainter than $\mu_R > 26$ mag arcsec^{-2} (Mihos et al. 2005; Zibetti et al. 2005). These are the regions of the stellar halos, where the ICL contribution increases with the distance from the center and is a part of the diffuse outer envelope (Zibetti et al. 2005; Gonzalez et al. 2007; Iodice et al. 2016; Spavone et al. 2017).

Simulations suggest that, during the hierarchical mass assembly of the galaxy clusters, the intracluster baryons build up from the tidal stripping of material from the outskirts of galaxies, through interaction and/or merging (Murante et al. 2007; Contini et al. 2014). Therefore, studying the main characteristics (i.e., distribution, colors, age, and metallicity) of the intracluster population constraint the progenitor galaxies and the processes at work in the formation of the cluster.

The detection and analysis of the intracluster component is really challenging, in particular for the ICL, due to its diffuse nature and very faint SB levels. In the last decade, deep data acquired over wide areas have increasingly contributed to our knowledge of the ICL properties. This component is mainly concentrated around the brightest galaxies and it is mapped out to several hundred kiloparsec from the center of the clusters (Zibetti et al. 2005; Gonzalez et al. 2007; Mihos et al. 2017). The fraction of stellar envelope plus the ICL around the BCG over the total light in the cluster (including galaxy members) is 10%–30% (Gonzalez et al. 2005; Zibetti et al. 2005; Seigar et al. 2007). The measured colors of the ICL are found to be similar to those of the major cluster galaxies, which is consistent with the hypothesis that this component could originate from interactions between them (Zibetti et al. 2005).

In the nearby universe, deep images of the Virgo cluster ($z \sim 0.004$) have revealed several faint ($\mu_V =$ 26–29 mag arcsec^{-2}) streams of ICL between the galaxy members, with the bulk detected close to the BCGs and colors $B - V = 0.7$–0.9 mag (Janowiecki et al. 2010; Capaccioli et al. 2015; Mihos et al. 2017). The total fraction of the ICL is ∼7%–10%. This value is smaller than that in massive and evolved clusters and could indicate that the ICL component in Virgo is still growing. Also in the Hydra I ($z \sim 0.01$) cluster, the ICL is still forming, since remnants of dwarf galaxies are identified in the outskirts of the central dominating galaxy NGC 3311 (Arnaboldi et al. 2012; Hilker et al. 2015).

At higher redshift ($z \sim 0.3$–0.5), the fraction of ICL decreases (5%–20% Giallongo et al. 2014; Montes & Trujillo 2014; Presotto et al. 2014), which is in agreement with theoretical predictions that suggest a late formation epoch for the intracluster population ($z < 1$ Murante et al. 2007; Contini et al. 2014).

In this paper, we present an unknown ICL region in the core of the Fornax cluster. This is the second most massive

galaxy concentration within 20 Mpc, after the Virgo cluster, where the mass assembly is still ongoing (Drinkwater et al. 2001; Scharf et al. 2005). Most of the bright ($m_B < 15$ mag) cluster members in the core are early-type galaxies (ETGs, Ferguson 1989). The Fornax cluster hosts a vast population of dwarf galaxies and ultra compact galaxies (Hilker 2015; Munoz et al. 2015; Schulz et al. 2016), an intracluster population of GCs (Bassino et al. 2006; Schuberth et al. 2010; D'Abrusco et al. 2016; Cantiello et al. 2017) and planetary nebulae (Napolitano et al. 2003; McNeil-Moylan et al. 2012).

In Fornax, a faint ($\mu_g \sim$ 29–30 mag arcsec^{-2}) stellar bridge of ICL, ∼29 kpc long, was found between NGC 1399 and NGC 1387 by Iodice et al. (2016). Based on the color analysis, it could result from the stripping of the outer envelope of NGC 1387 on its east side. Such a feature was already detected in the spatial distribution of the blue GCs (Bassino et al. 2006; D'Abrusco et al. 2016).

In this paper, we aim to estimate the total luminosity and colors of the newly discovered ICL in Fornax (in Sections 3–5) and to discuss its origin (Section 6).

2. Data: The FDS with VST

This work is based on the Fornax Deep Survey (FDS) data presented by Iodice et al. (2016). FDS is a multiband (u, g, r, and i) imaging survey, obtained with the European Southern Observatory (ESO) Very Large Telescope Survey Telescope (VST), which covers 26 square degrees around the central galaxy NGC 1399 of the Fornax cluster (see Iodice et al. 2016, 2017; Venhola et al. 2017). The limiting 5σ magnitudes (in AB system) for 1 arcsec^2 area are 27.6, 28.5, 28.5, and 27.1 mag in the u, g, r, and i bands, respectively.

VST is a 2.6 m wide field optical survey telescope, located at Cerro Paranal in Chile (Schipani et al. 2012), equipped with the wide field camera (1×1 degree^2) OmegaCam, and has a pixel scale of 0.21 arcsec pixel^{-1}.

Data reduction was performed using the VST-Tube pipeline (Grado et al. 2012; Capaccioli et al. 2015) and the analysis was described in detail by Iodice et al. (2016). The "step-dither" observing strategy, adopted for the FDS, allows a very accurate estimate of the sky background (Iodice et al. 2016, 2017). In particular, the average sky frame derived for each observing night takes into account the small contribution to the sky brightness by the smooth components (i.e galactic cirrus, zodiacal light, and of the terrestrial airglow) plus the extragalactic background light. In the sky-subtracted science frame, only a possible differential component could remain, which contributes to the "residual fluctuations" in the background and sets the accuracy of the sky-subtraction step.

In this work, we analyzed the core of the Fornax cluster (see the left panel of Figure 1) from the g- and r-band mosaics. We adopt a distance for NGC 1399 of $D = 19.95$ Mpc (Tonry et al. 2001), therefore the image scale is 96.7 parsecs arcsec^{-1}.

3. Map of the Diffuse ICL

On the west side of the Fornax cluster, close to the NGC 1399 in the core, we detect several patches of diffuse light in the intracluster region (see the right panel of Figure 1). These features are very faint, with a r-band SB $\mu_r \simeq$ 28–29 mag arcsec^{-2}. They extend out to about 40 arcmin (∼230 kpc) from the center of NGC 1399 and over an area of about 430 arcmin^2, in the east-west direction for $-97° \leqslant$ P.A. $\leqslant -56°$. The bulk of the ICL is concentrated between the three bright ETGs in the core: NGC 1387, NGC 1379, and NGC 1381. The dwarf elliptical FCC 182 is completely embedded in this diffuse over-density of light.

In order to map the ICL and derive the integrated magnitudes and $g - r$ colors, we subtract a 2D model of the light distribution of all ETGs in the area, including NGC 1399. The right panel of Figure 1 shows the residual image. For each galaxy, the 2D model results from the isophotal analysis made using the Image Reduction and Analysis Facility (IRAF) task ELLIPSE. It takes into account the azimuthally averaged SB distribution, as well as the ellipticity and position angle (P.A.) variations as a function of the semimajor axis, down to the average background level in that field. A detailed description of the adopted method is available in Iodice et al. (2016), which is a similar approach to that adopted from other studies on the ICL in clusters (e.g., Krick & Bernstein 2007).

Figure 2 shows the azimuthally-averaged SB profiles for the three brightest ETGs (NGC 1387, NGC 1379, and NGC 1381) close to the ICL region, derived by the isophote fit; they extend out to 4–9 arcmin (∼23–50 kpc) from the galaxy center and map the light down to the faintest of the galaxy's outskirts ($\mu_r \simeq$ 29 mag arcsec^{-2}), i.e., to the region of the stellar halos. The 2D model made for each ETG reproduces the whole galaxy light distribution,[11] including the stellar halo (shown in Figure 2), and takes into account the variations in the ellipticity and P.A. (shown in Figures 4 and 5). By subtracting the 2D model derived from the above analysis for each galaxy, the residual image clearly shows an excess of light in the intracluster region between the three bright ETGs in the core (see the right panel of Figure 1). Moreover, the residual image allows us to detect some other patches of ICL on the northwest side, between NGC 1381 and NGC 1380B, between NGC 1381 and NGC 1374; and in the south, between NGC 1399 and NGC 1389 (see the right panel of Figure 1). They appear as bridge-like structures connecting the galaxies.

As pointed out in previous studies on ICL (Gonzalez et al. 2005; Zibetti et al. 2005; Krick & Bernstein 2007; Rudick et al. 2011; Montes & Trujillo 2017), the separation of the ICL from the extended stellar halo in BCGs is a tricky task since the two components tend to merge at the faintest SB levels and therefore, it is hard to uniquely separate each contribution by deep photometry alone. In the isophotal analysis we performed for the ETGs close to ICL region maps, the SB out to the very faintest galaxy outskirts, therefore the 2D model made for each galaxy reproduce it out the region of the stellar halos. Here the fit could include also a small fraction of the ICL, which is mixed with the stellar bounded component. Alternatively, if the outskirts of galaxies deviate in shape from pure ellipses, they would appear as substructures in the residual map and can contribute to the ICL. In Fornax, this is the case for NGC 1379 and NGC 1387. The outer isophotes of NGC 1379 are quite extended on the west-northwest side, suggesting that this galaxy could have a

[11] The bright residuals in the inner regions of NGC 1387 and NGC 1381 are due to the presence of substructures, like an inner bar and dust in NGC 1387, and a boxy bulge and thick disk in NGC 1381. The discussion of such a features, which do not affect the ICL geometry and fraction, is out of the scope of the present work; they will be analyzed in detail in a forthcoming paper (E. Iodice et al. 2017, in preparation).

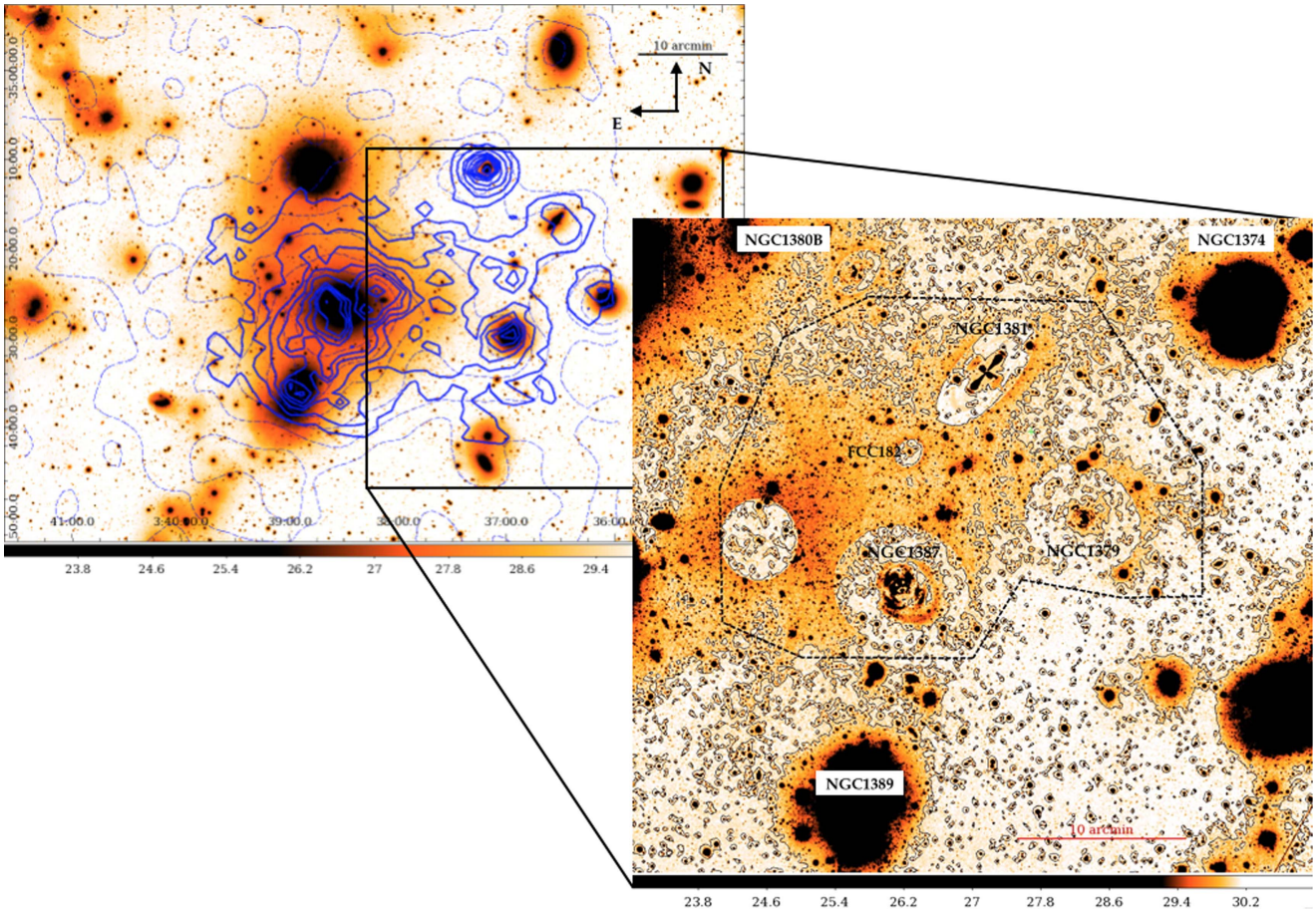

Figure 1. Left panel—central regions (2×1 degrees^2) of the Fornax cluster in the r-band surface brightness levels. The blue contours are the spatial distribution of the blue GCs derived by D'Abrusco et al. (2016; solid lines) and by Cantiello et al. (2017; dashed lines). Right panel—enlarged regions on the west side (40.9×42.7 arcmin $\sim 237 \times 248$ kpc), where the bright galaxies were modeled and subtracted. In this area, the diffuse ICL is the central over-density that fills the intracluster space. The black contours are the surface brightness levels $\mu_r = 29.8$–30.02 mag arcsec^{-2}. The black dashed region marks the polygon aperture used to measure the integrated magnitudes of the ICL (see Section 3.1).

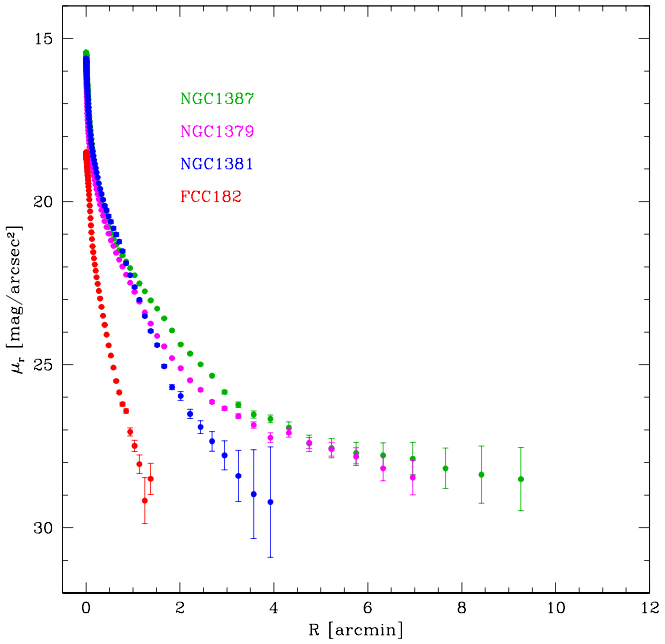

Figure 2. Azimuthally averaged surface brightness, in the r band, for the three brightest ETGs (NGC 1387, NGC 1379, and NGC 1381) and for the dwarf elliptical FCC 182 close to the ICL region.

very asymmetric stellar halo that is elongated in the opposite direction of the ICL (see Figure 4, top panel). Something similar was observed for NGC 1387, whose outer isophotes extend on the west-northwest side (see Figure 4, bottom panel), which is opposite to the region where the bridge of light toward NGC 1399 is detected (Iodice et al. 2016).

In any case, even taking into account the uncertainties in the 2D models of the galaxies at the faintest levels, we are confident that the detected ICL in the core of the Fornax cluster does not result from the overlap along the line of sight of the galaxies extended stellar halos, but it is a real additional diffuse component in this intracluster region. In fact, we found that the distance from the center of each object to the bulk of the ICL is between 10 and 15 arcmin, which is larger than the maximum semimajor axis reached by the surface photometry ($R \sim 4$–9 arcmin; see Figure 2).

3.1. Magnitudes and Colors of the ICL

We derived the total magnitudes in the g and r bands integrated over an area of $\sim$432 arcmin^2, covering the bulk of the ICL. We used the IRAF tasks POLYMARK to trace a polygon including the intracluster region between NGC 1387, NGC 1379, NGC 1381, and NGC 1380B, and POLYPHOT to estimate the integrated magnitude inside this area. Foreground

and background points and extended sources (stars and galaxies) were masked and excluded from the flux estimate. We account for an average value of the "local" residual background level 12, and the error estimate on the total magnitudes takes into account the scatter in the background level, as also described in Iodice et al. (2016).

Magnitudes are corrected for the Galactic extinction (using $A_g = 0.042$ and $A_r = 0.029$, Schlegel et al. 1998) and they are $m_g^{\rm ICL} = 12.1 \pm 0.3$ mag and $m_r^{\rm ICL} = 11.4 \pm 0.3$ mag. Therefore, the total luminosity in the g band is $L_g \simeq 8.3 \times 10^9\ L_\odot$ ($L_V \simeq 7 \times 10^9\ L_\odot$, since $g - V = 0.39$ from Fukugita et al. 1996). The fraction of ICL, with respect to the total luminosity of NGC 1399 ($L_g \simeq 1.66 \times 10^{11}\ L_\odot$, see Iodice et al. 2016), is about 5%. Compared only to the outer extended stellar envelope of NGC 1399, the fraction of the ICL is about 7%.

The $g - r$ integrated color of the ICL is 0.7 ± 0.4 mag ($B - V \sim 0.85$ mag). Over the whole extension of the ICL, for $10 \leqslant R \leqslant 45$ arcmin, we estimate that the color varies in the range $0.6 \leqslant g - r \leqslant 1.4$ mag ($B - V = 0.79$–1.55 mag). These values are comparable with the $g - r$ colors in the outskirts of the three ETGs close to the ICL region, which are $g - r \sim 0.6$ mag for NGC 1381, $g - r \sim 0.8$–1.5 mag for NGC 1379, and $g - r \sim 0.8$–1 mag for NGC 1387 (E. Iodice et al. 2017, in preparation). The stellar halo of NGC 1399 also has a similar color of $g - r \sim 0.8$ mag (Iodice et al. 2016).

4. ICL versus Intracluster GCs

From the FDS *ugri* images covering the central $\sim$8.4 deg^2 of the cluster, D'Abrusco et al. (2016) traced the spatial distribution of candidate GCs in a region $\sim$0.5 deg^2 within the core of the Fornax cluster. The density contours of blue GCs are over-plotted to the light distribution (see Figure 1, left panel). D'Abrusco et al. (2016) pointed out that the blue GCs density map is elongated on the east-west direction, as also found for the the light distribution (Iodice et al. 2016), and an over-density of blue GCs is found between NGC 1381, NGC 1379, and NGC 1380B (see also Bassino et al. 2006). This over-density correlates with the area where the bulk of ICL is detected (see Section 3). Besides, the blue GCs on NGC 1379 are more concentrated on the east side, falling in the same intracluster region. There is a strong correlation also between the distribution of blue GCs and the other detected bridge-like structure of ICL; the blue GCs around NGC 1380B appear more elongated toward the south, as is the diffuse light, and an over-density of blue GCs is found into intracluster region between NGC 1389 and NGC 1387 (see Figure 1, left panel).

We estimate that the over-density of blue GCs in the northwest region, where the total magnitude of the ICL is derived (i.e., $R \leqslant 45$ arcmin, see Section 3), is $\sim$4% of the total population of blue GCs of NGC 1399 alone, so all GCs that should be associated to the halos of other galaxies in the core are not counted in. To do this, we assume that the GCs to not be considered are all candidates inside the outer isophote tracing the stellar halo.

[12] The residual fluctuations in the sky-subtracted images are the deviations from the background in the science frame, with respect to the average sky frame obtained by the empty fields close to the target. Therefore, by estimating them, we obtain an estimate on the accuracy of the sky-subtraction step. See Iodice et al. (2016) for a detailed description of this approach.

The above results are further confirmed by the spatial distribution of the blue GCs derived by Cantiello et al. (2017) from the same FDS data (see the blue dashed contours in Figure 1). By adopting less stringent selection constraints, the new sample is larger (almost double) and includes all GCs already mapped by D'Abrusco et al. (2016). Using the new GC catalog, the over-density of blue GCs in the northwest region of ICL increases to $\sim$7%. Both estimates are comparable with the fraction of ICL ($\sim$5%).

The correspondence of the spatial and fraction of the over-densities of blue GCs with the newly detected ICL over different patches is a strong indication of intracluster stellar populations in the core of the Fornax cluster.

5. Radial Distribution of the Intracluster Components

To analyze the radial distribution of the ICL, we derived the average SB profiles in a cone of 40° wide (for $-97° \leqslant$ P.A. $\leqslant -56°$), centered on NGC 1399, from (i) the residual g and r-band images, where ETGs in this area are subtracted (except NGC 1399); and (ii) from the same images where also NGC 1399 is modeled and subtracted. In both cases, all bright foreground stars and background objects were accurately masked. We also derived SB profiles on the southeast side for $83° \leqslant$ P.A. $\leqslant 124°$, which is the region opposite of the ICL with respect to NGC 1399. Results are shown in Figure 3. On the northwest side, the SB extends out to 45 arcmin ($\sim$260 kpc) from the center of the Fornax cluster. Light from the stellar envelope of NGC 1399 ($R \geqslant 10$ arcmin Iodice et al. 2016) dominates the SB profiles out to $R \sim 20$ arcmin, where all profiles in both bands are consistent with each others. At larger radii, the g and r light profiles in the northwest show an excess of light ($\mu \sim 28$–29 mag arcsec^{-2}). In the g band, this is about one magnitude brighter than both the azimuthally averaged values and that on the southeast side at the same radius. In the r band, extra-light is detected where the azimuthally averaged profile in the southeast cone have no significant detection.

Asymmetries in the light distributions with respect to the average were already discussed in Iodice et al. (2016). The light profiles extracted along several position angles show an excess of light on the west side of NGC 1399, where the bulk of ICL is found. The most significant intracluster region is that in between NGC 1387, NGC 1379, and NGC 1381 ($15 \leqslant R \leqslant 30$ arcmin), at P.A. $= 98°$ west, where $27 \leqslant \mu_g \leqslant 28$ mag arcsec^{-2}, which is two magnitudes brighter than the light at the corresponding radii on the east side (see Figure 9 of Iodice et al. 2016).

By subtracting also the light from NGC 1399, we can trace the ICL at smaller radii than those given above, i.e., $10 \leqslant R \leqslant 30$ arcmin (see the right panel of Figure 1), were the it is completely blended by the light in the stellar halo of NGC 1399. For $-97° \leqslant$ P.A. $\leqslant -56°$, it has an almost constant profile, with $\mu_g \sim 26.6$ mag arcsec^{-2} and $\mu_r \sim 27.2$ mag arcsec^{-2}, showing a maximum for $10 \leqslant R \leqslant 20$ arcmin (see the left panel Figure 3). This region corresponds to the bulk of the ICL (see Section 3). On the southeast side ($83° \leqslant$ P.A. $\leqslant 124°$), there is no detection above the background level.

Similar to the analysis of the SB profiles, we estimated the number of blue GCs inside the same areas where SB profiles are derived (i.e., NW $-97° \leqslant$ P.A. $\leqslant -56°$ and SE $83° \leqslant$ P.A. $\leqslant 124°$ cones). The GCs were selected in each SB level as function of the radius (see the right panel of Figure 3). This was done for

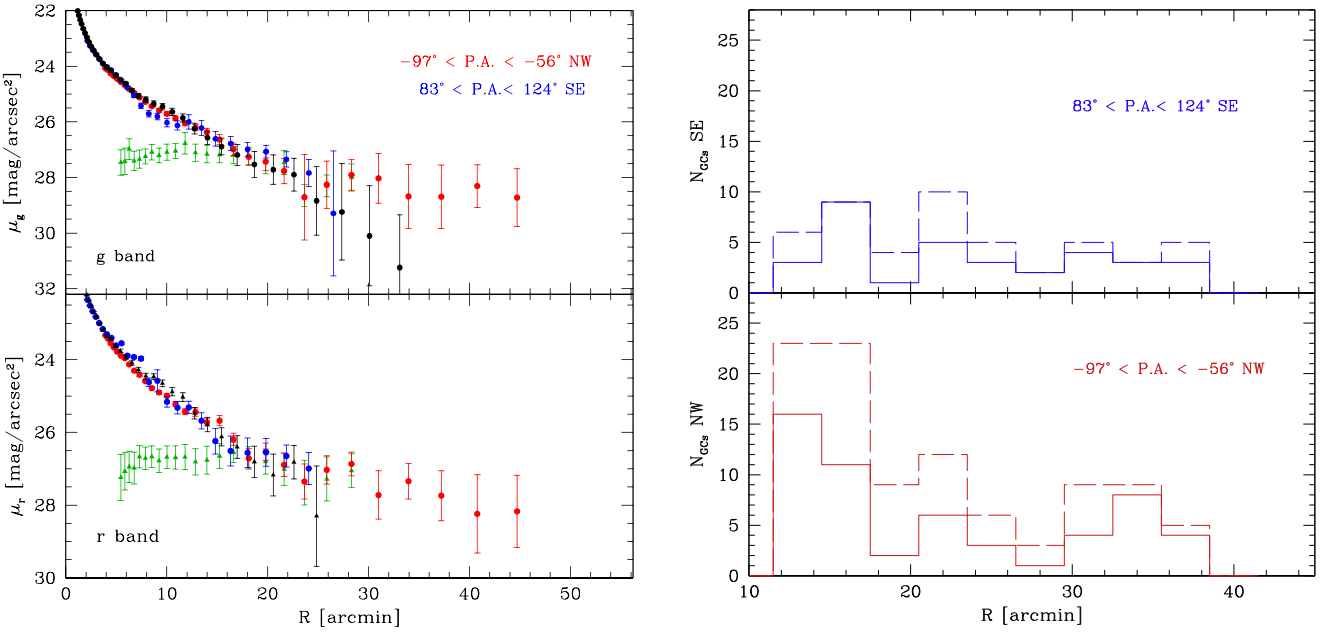

Figure 3. Left panel—SB profiles in the g (upper panels) and r bands (bottom panels), extracted in different areas around NGC 1399. Red circles: SB for $-97° \leqslant$ P.A. $\leqslant -56°$, which covers the ICL region. Blue circles: SB for $83° \leqslant$ P.A. $\leqslant 124°$, which is the region opposite of the ICL with respect to NGC 1399. Black circles: azimuthally averaged SB profiles derived by Iodice et al. (2016). Red triangles: SB distribution of the ICL for $-97° \leqslant$ P.A. $\leqslant -56°$ derived on the image where the light from NGC 1399 is subtracted. Right panel—the number of blue GCs inside the northwest (red lines, bottom panel) and southwest (blue lines, upper panel) regions where the surface brightness profiles are extracted (left panels) for the sample studied by D'Abrusco et al. (2016; solid line) and Cantiello et al. (2017) (dashed line).

both samples of blue GCs, by D'Abrusco et al. (2016) and Cantiello et al. (2017). On average, the blue GC distribution is almost constant with radius on the SE, while there are two peaks on the northwest: one at $10 \leqslant R \leqslant 20$ arcmin, where the bulk of ICL is detected and another for $R \geqslant 30$ arcmin where we observe an extra-light from the SB profiles.

6. Discussion: What is the Origin of the Intracluster Population?

In the core of the Fornax cluster, on the west side of NGC 1399, we detected a previously unknown region of ICL (see the right panel of Figure 1). The bulk of ICL is between the three bright ETGs in the core, NGC 1387, NGC 1379, and NGC 1381, at $10 \leqslant R \leqslant 40$ arcmin (∼58–230 kpc) from the center of NGC 1399. The ICL is therefore confined in a small area (∼1%) compared to the total extension of the Fornax cluster.

One of the major results of this work is the spatial coincidence and fraction of the over-densities of blue GCs with the newly detected ICL over different patches. We found that the ICL is the counterpart in the diffuse light of the over-density in the blue intracluster GCs detected by D'Abrusco et al. (2016). The ICL in this region of the cluster amounts to ∼5% of the total light of the brightest cluster member NGC 1399. This turns also to be consistent with the fraction of blue GCs (∼4%–6%) with respect to the total population of blue GCs, in the same area. The above findings are a strong indication for intracluster stellar populations in the core of the Fornax cluster.

The ICL in the core of the Fornax cluster shows similar properties to the ICL detected in other clusters of galaxies. Its total luminosity in the V band is $L_V \simeq 7 \times 10^9\ L_\odot$ (see Section 3). It is comparable with the total luminosity of several streams of ICL found in the Virgo cluster, around the BCGs, which are in the range $2.3 \leqslant L_V \leqslant 5.6 \times 10^9\ L_\odot$ (Janowiecki et al. 2010; Mihos et al. 2017). The ICL integrated color is $g - r \sim 0.7$ mag (see Section 3), corresponding roughly to $B - V \sim 0.85$ mag. This is comparable to the $B - V$ colors derived for the ICL streams in the Virgo cluster (Mihos et al. 2017), which are in the range 0.7–0.9 mag, and it is also consistent with the $g - r = 0.68$ mag found for the ICL in Abell cluster A2744 from Montes & Trujillo (2014). From SB profiles, the ICL colors for $10 \leqslant R \leqslant 45$ arcmin are in the range $0.6 \leqslant g - r \leqslant 1.4$ mag ($B - V = 0.79$–1.55 mag). These are consistent with $g - r \simeq 1$–1.2 mag found for the ICL in clusters from Zibetti et al. (2005).

Theoretical studies on mass assembly and ICL formation indicate that the morphology and evolution over time strongly depend on the processes at work and on the environment. In particular, the main mechanism able to produce the intracluster population is the stripping of material from galaxies, which could happen during the initial collapse of the cluster (Merritt 1984) or could be induced by the cluster potential (Byrd & Valtonen 1990; Gnedin 2003) and/or from the high-speed encounters between cluster members (Mihos 2004; Rudick et al. 2006). During the cluster evolution, all these processes can contribute to the formation of the ICL at different epochs and/or in different regions of the cluster. Using N-body simulations, Rudick et al. (2009) modeled the ICL formation and studied the morphology and evolution of this component. Their main results suggest that: (i) the morphology depends on the mechanism that has produced the ICL, i.e., long streams and tails form during the merging of

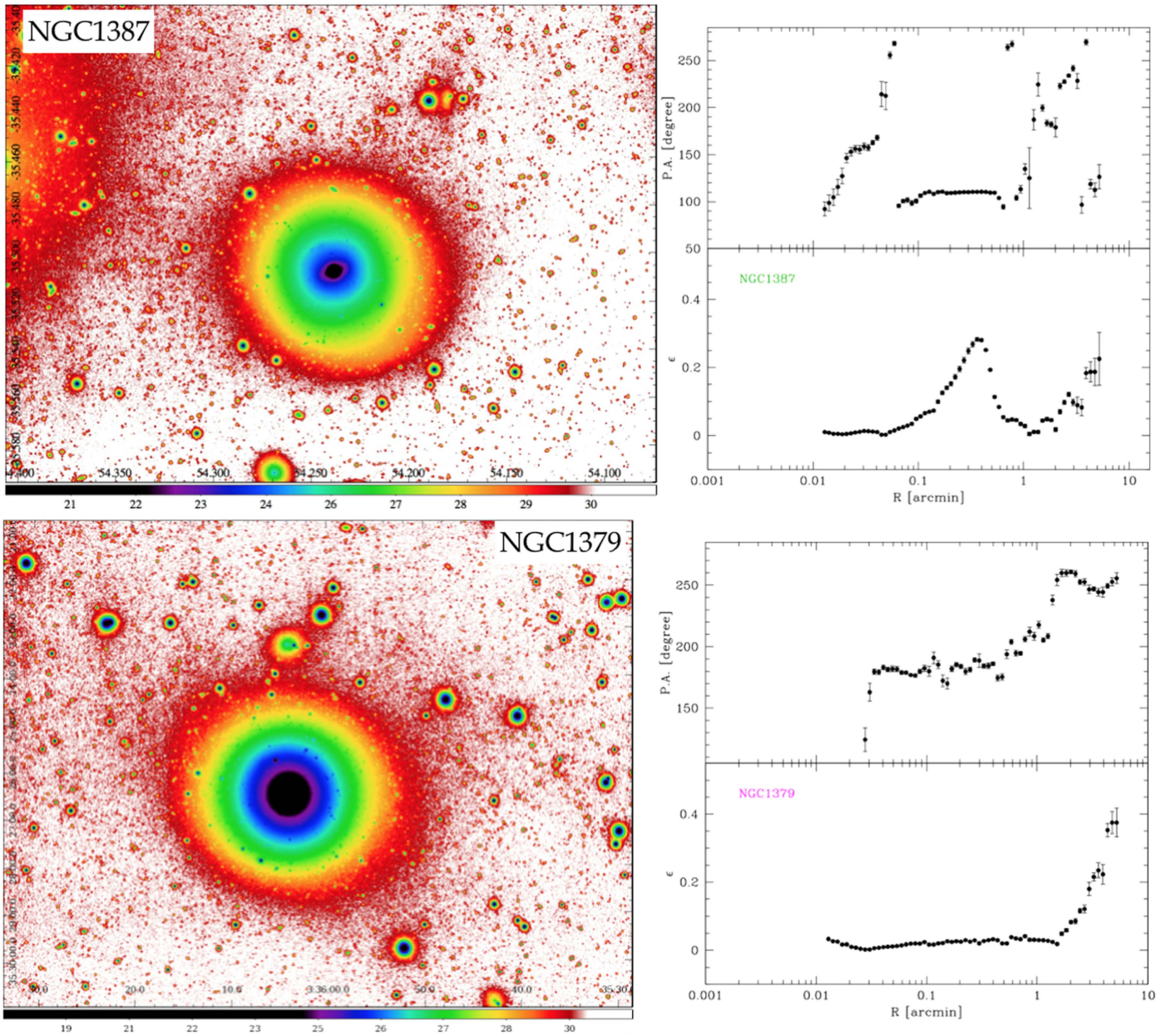

Figure 4. Extracted images from the *r*-band VST mosaic of the core of the Fornax cluster, as shown in Figure 1, around the galaxy NGC 1387 (top left panel) and NGC 1379 (bottom left panel). Images are shown in surface brightness levels reported in the color bar on the bottom. On the right panels, the ellipticity (top) and P.A. (bottom) profiles are shown, as function of the semimajor axis, and are derived by fitting the isophotes in the *r*-band images.

galaxies, while a close encounter of a galaxy with the central brightest galaxy (cD) tends to form shapeless structures like shells or plumes; and (ii) the evolution is a function of the cluster potential, i.e., once the ICL is formed, its decay time is ∼1.5 times the dynamical time in the cluster, before fading into a smooth component. This means that in evolved clusters of galaxies, the ICL is in a more diffuse form within the cluster, while in an early stage formation, the ICL appears as long and linear streams.

The qualitative model predictions can be contrasted to our observational findings to constraint the formation history of the intracluster component (light and GCs) in the core of the Fornax cluster. The "observables" are: (i) the morphology of the ICL and (ii) its location in the cluster. The ICL in Fornax is in the form of faint and diffuse patches, concentrated between the cD (NGC 1399) and the three bright ETGs, NGC 1387, NGC 1379, and NGC 1381 (see the right panel of Figure 1), for $R \leqslant 58$–230 kpc, which is within the cluster core and well inside the the virial radius ($R_{\rm vir} \sim 700$ kpc). Compared with the simulations by Rudick et al. (2009), the above properties of the ICL are consistent with the scenario where this component formed by stripped material from the outskirts of a galaxy in a close passage with the cD. If any stream formed in the core of the cluster it was destroyed within few Gyr by the strong tidal field of the cluster in this region. Therefore, as Fornax is likely to be dynamically evolved cluster, one would expect to see a rather smooth ICL component than distinct streams in its core. Our findings are consistent with this expectation.

The bright galaxy NGC 1404, which is close in projection to NGC 1399 on the southeast (see the left panel of Figure 1), but with a velocity difference of $\sim$500 km s^{-1} to NGC 1399, could have contributed to form such a region of intracluster population with stripped material from its outskirt in passages close to NGC 1399 (Bekki et al. 2003). But the other ETGs galaxies close to the ICL regions, as NGC 1381, which has a velocity difference of $\sim$300 km s^{-1} far ($V \sim 1724$ km s^{-1}) to NGC 1399 ($V \sim 1425$ km s^{-1}), and NGC 1379 ($V \sim 1324$ km s^{-1}) and NGC 1387 ($V \sim 1302$ km s^{-1}), could have contributed to the growth of the ICL via tidal interactions with the cluster potential. Such a process was invoked to explain the origin of the stellar bridge connecting NGC 1399 and NGC 1387 (Iodice et al. 2016), which is part of this ICL region. This scenario is further supported by finding that two of the major galaxies in the ICL region (NGC 1387 and NGC 1379) have a lopsided stellar halo (see Figure 4), indicating gravitational displacements via tidal interaction, with average colors of $0.6 \leqslant g - r \leqslant 1.5$ mag that are comparable with the average value estimated for the ICL in Fornax (see Section 5).

Even if the analysis performed and discussed in this paper suggests that the intracluster population (GCs and diffuse light) in the core of the Fornax cluster could origin from the outskirts of the galaxies in this region, for the sake of completeness, we mention below any other possible formation process for this component.

A fraction of the ICL population in this region of the cluster could also come from lower-mass dwarf galaxies that are tidally disrupted in the potential well of the massive galaxies. This is supported by a recent study from Venhola et al. (2017) that found a drop in the number density of LSB galaxies at cluster-centric distances smaller than $\sim$180 kpc inward.

The blue GCs found in the region of the ICL have a typical $g - r \sim 0.5$ mag (D'Abrusco et al. 2016) bluer than the diffuse light. This is expected, since specific frequencies of the blue (old and metal-poor) GCs are higher in the outer halos of galaxies, whereas the stellar population might be, on average, redder and more metal-rich (Lamers et al. 2017, and reference therein). This would also indicate that GCs might come from less massive and hence less metal-rich disrupted LSB galaxies, since the specific frequency of GCs strongly increases toward lower-luminosity dwarf galaxies (Peng et al. 2008).

As conclusive remark, we stress that the spatial coincidence of the ICL with the GCs found in the core of the Fornax cluster turned out a really powerful tool to trace the intracluster baryons and therefore, to study the formation and evolution of this component. If the same analysis is performed on other clusters of galaxies and the same coincidence is still found, then this would suggest that 2D maps of GCs could be considered as a valid alternative to the light distribution maps to study the intracluster population. This perspective should be more properly considered in the era of the new generation of large telescopes and adaptive optics, since they could provide an easier detection of the intracluster compact sources rather than of the diffuse light, which requires tricky tasks for data reduction and analysis.

This work is based on visitor mode observations taken at the ESO La Silla Paranal Observatory within the VST GTO Program ID 094.B-0496(A). The authors wish to thank the anonymous referee for his/her comments and suggestions that allowed us to greatly improve the paper. Authors acknowledges financial support from the INAF VST funds and wish to thank ESO for the financial contribution given for the visitor mode runs at the ESO La Silla Paranal Observatory. The authors acknowledges financial support from the European Unions Horizon 2020 research and innovation program under the Marie Skodowska-Curie grant agreement No. 721463 to the SUNDIAL ITN network. N.R.N. and E.I. received support within PRIN INAF 2014 "Fornax Cluster Imaging and Spectroscopic Deep Survey." G.VdV. acknowledges partial support from Sonderforschungsbereich SFB 881 "The Milky Way System" (subprojects A7 and A8) funded by the German Research Foundation.

Appendix
Images of the Galaxies Close to the ICL Region

In this section, we show the images of the three bright ETGs in the core of the Fornax cluster, NGC 1387, NGC 1379 (see Figure 4), and NGC 1381 (Figure 5, top panel); and of the dwarf elliptical FCC 182 (Figure 5, bottom panel), which is completely embedded in this diffuse over-density of light (see Figure 1). These are in SB levels in the r band and were extracted from the whole VST mosaic shown in Figure 1. In the right panels of Figures 4 and 5, we show the ellipticity and P.A. profiles, as function of the semimajor axis, derived by fitting the isophotes in the r-band images.

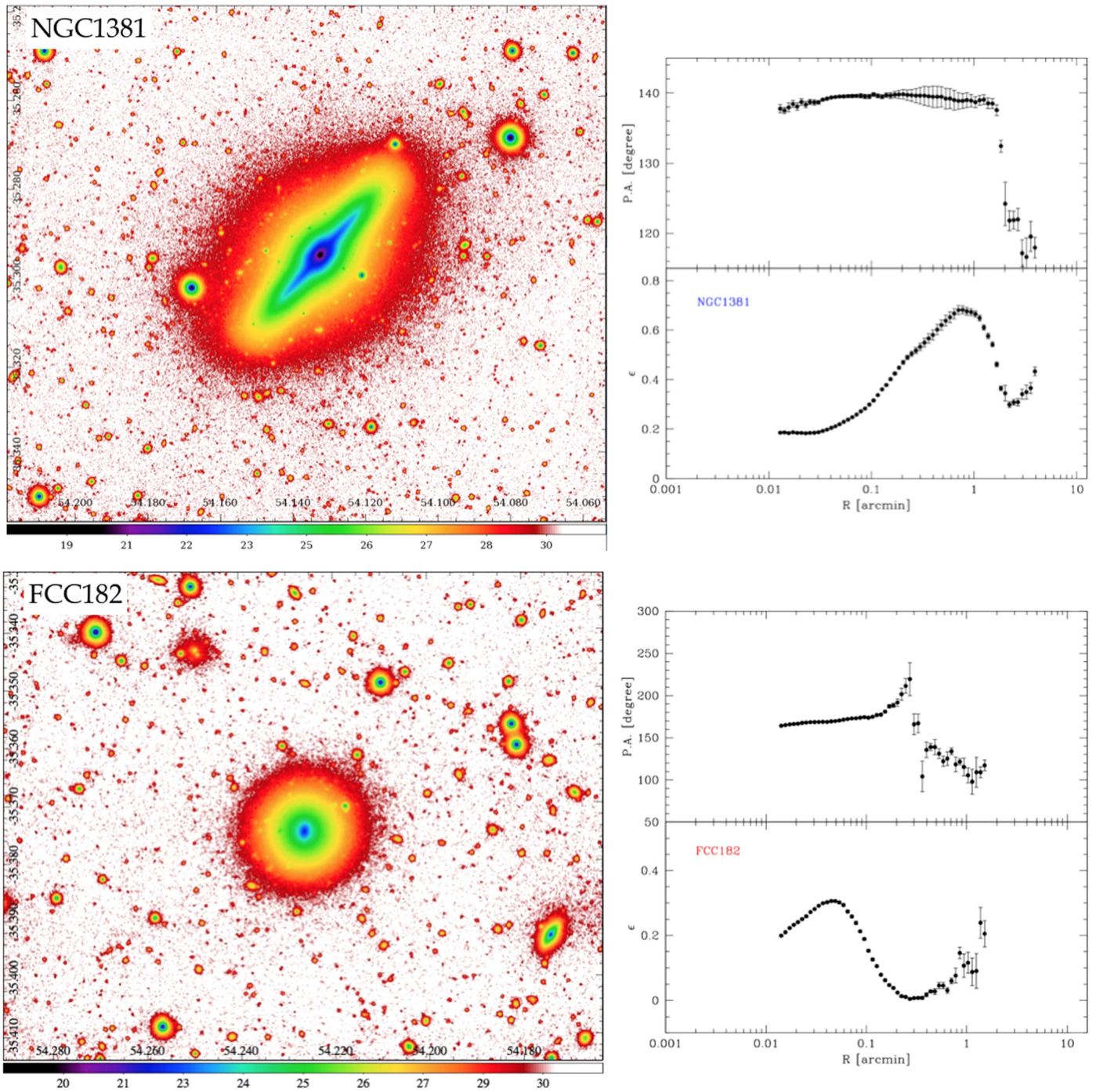

Figure 5. Same as Figure 4 for the S0 galaxy NGC 1381 (top panels) and for the dwarf elliptical FCC 182 (bottom panels).

ORCID iDs

E. Iodice https://orcid.org/0000-0003-4291-0005
M. Spavone https://orcid.org/0000-0002-6427-7039
M. Cantiello https://orcid.org/0000-0003-2072-384X
R. D'Abrusco https://orcid.org/0000-0003-3073-0605
R. F. Peletier https://orcid.org/0000-0001-7621-947X
L. Limatola https://orcid.org/0000-0002-1896-8605
A. Grado https://orcid.org/0000-0002-0501-8256
M. Paolillo https://orcid.org/0000-0003-4210-7693
P. Schipani https://orcid.org/0000-0003-0197-589X

References

Arnaboldi, M., & Gerhard, O. 2010, HiA, 15, 97
Arnaboldi, M., Ventimiglia, G., Iodice, E., et al. 2012, A&A, 545, 37
Bassino, L. P., Faifer, F. R., Forte, J. C., et al. 2006, A&A, 451, 789
Bekki, K., Forbes, D. A., Beasley, M. A., et al. 2003, MNRAS, 344, 1334
Byrd, G., & Valtonen, M. 1990, ApJ, 350, 89
Cantiello, M., D'Abrusco, R., Spavone, M., et al. 2017, A&A, in press (arXiv:1711.00750)
Capaccioli, M., Spavone, M., Grado, A., et al. 2015, A&A, 581, 10
Contini, E., De Lucia, G., Villalobos, Á, et al. 2014, MNRAS, 437, 3787
D'Abrusco, R., Cantiello, M., Paolillo, M., et al. 2016, ApJL, 819, L31
Drinkwater, M. J., Gregg, M. D., & Colless, M. 2001, ApJL, 548, L139

Ferguson, H. C. 1989, AJ, 98, 367
Fukugita, M., Ichikawa, T., Gunn, J. E., et al. 1996, AJ, 111, 1748
Giallongo, E., Menci, N., Grazian, A., et al. 2014, ApJ, 781, 24
Gnedin, O. Y. 2003, ApJ, 582, 141
Gonzalez, A. H., Zabludoff, A. I., & Zaritsky, D. 2005, ApJ, 618, 195
Gonzalez, A. H., Zaritsky, D., & Zabludoff, A. I. 2007, ApJ, 666, 147
Grado, A., Capaccioli, M., Limatola, L., et al. 2012, MSAIS, 19, 362
Hilker, M. 2015, IAUGA, 22, 2215712
Hilker, M., Barbosa, C. E., Richtler, T., et al. 2015, in IAU Symp. 309, Galaxies in 3D Across the Universe, ed. B. L. Ziegler, F. Combes, H. Dannerbauer & M. Verdugo (Cambridge: Cambridge Univ. Press), 221
Iodice, E., Capaccioli, M., Grado, A., et al. 2016, ApJ, 820, 42
Iodice, E., Spavone, M., Capaccioli, M., et al. 2017, ApJ, 839, 21
Janowiecki, S., Mihos, J. C., Harding, P., et al. 2010, ApJ, 715, 972
Krick, J. E., & Bernstein, R. A. 2007, AJ, 134, 466
Lamers, H. J. G. L. M., Kruijssen, J. M. D., Bastian, N., et al. 2017, A&A, 606, A85
McNeil-Moylan, E. K., Freeman, K. C., Arnaboldi, M., et al. 2012, A&A, 539, 11
Merritt, D. 1984, ApJ, 276, 26
Mihos, J. C. 2004, in IAU Symp. 217, The Evolution of Tidal Debris, ed. P.-A. Duc, J. Braine, & E. Brinks (Cambridge: Cambridge Univ. Press), 390
Mihos, J. C. 2015, IAUGA, 29, 2247903
Mihos, J. C., Harding, P., Feldmeier, J., et al. 2005, ApJL, 631, L41
Mihos, J. C., Harding, P., Feldmeier, J. J., et al. 2017, ApJ, 834, 16
Montes, M., & Trujillo, I. 2014, ApJ, 794, 137
Montes, M., & Trujillo, I. 2017, MNRAS, in press (arXiv:1710.03240)
Munoz, R. P., Eigenthaler, P., Puzia, T. H., et al. 2015, ApJL, 813, L15
Murante, G., Giovalli, M., Gerhard, O., et al. 2007, MNRAS, 377, 2
Napolitano, N. R., Pannella, M., Arnaboldi, M., et al. 2003, ApJ, 594, 172
Peng, E. W., Jordán, A., & Côté 2008, ApJ, 681, 197
Presotto, V., Girardi, M., Nonino, M., et al. 2014, A&A, 565, 126
Rudick, C. S., Mihos, J. C., Frey, L. H., et al. 2009, ApJ, 699, 1518
Rudick, C. S., Mihos, J. C., & McBride, C. 2006, ApJ, 648, 936
Rudick, C. S., Mihos, J. C., McBride, C. K., et al. 2011, ApJ, 732, 48
Scharf, C. A., Zurek, D. R., & Bureau, M. 2005, ApJ, 633, 154
Schipani, P., Noethe, L., Arcidiacono, C., et al. 2012, JOSAA, 29 1359
Schlegel, D. J., Finkbeiner, D. P., & Davis, M. 1998, ApJ, 500, 525
Schuberth, Y., Richtler, T., Hilker, M., et al. 2010, A&A, 513, 52
Schulz, C., Hilker, M., Kroupa, P., et al. 2016, A&A, 594, 119
Seigar, M. S., Graham, A. W., & Jerjen, H. 2007, MNRAS, 378, 1575
Spavone, M., Capaccioli, M., Napolitano, N. R., et al. 2017, A&A, 603, A38
Tonry, J. L., Dressler, A., Blakeslee, J. P., et al. 2001, ApJ, 546, 681
Tutukov, A. V., & Fedorova, A. V. 2011, ARep, 55, 383
Venhola, A., Peletier, R. P., Laurikainen, E., et al. 2017, A&A, in press (arXiv:1710.04616)
Zibetti, S., White, S. D. M., Schneider, D. P., et al. 2005, MNRAS, 358, 949